Original scientific paper

Role of the newly synthesized brightener in modification of surface properties of Zn-Ni alloy electrodeposited on steel substrate

Jyoti S. Kavirajwar[a], Basavanna Shivarudraiah[b, ✉], Yanjerappa Arthoba Nayaka[c]

[a]*Department of Chemistry, The Oxford College of Engineering, Bangalore-560068, Karnataka, India*
[b]*Department of Chemistry, BTL Institute of Technology & Management, Bangalore-560099, Karnataka, India*
[c]*Department of Chemistry, Kuvempu University, Shankaraghatta, Shimoga-577451, Karnataka, India*

Corresponding author: ✉drsbasavanna@gmail.com; Tel.: +91 9901984626

Abstract

In the present study, a new brightener was synthesized by condensation of salicylaldehyde and cysteine hydrochloride (SC). To examine the influence of SC on the nucleation mechanism of Zn-Ni alloy, electrodeposition, cyclic voltammetric and chronoamperometric studies were carried out. The model of Schariffker and Hills was used to analyze current transients which explained the electrocrystallization process of Zn-Ni alloy. It is revealed that Zn-Ni electrocrystallization process in presence of SC is regulated by instantaneous nucleation mechanism. The corrosion studies were done for the bright and dull zinc-nickel alloy coatings in 3.5 wt.% NaCl solution, using potentiodynamic polarization and electrochemical impedance spectroscopic techniques. The phase structure, surface morphology and brightness of the deposit were characterized by means of X-ray diffraction (XRD) analysis, scanning electron microscopy (SEM) and reflectance studies. These studies revealed the role of SC in producing a bright Zn-Ni alloy coating on mild steel substrate and also showed its improved corrosion resistant nature.

Keywords

Nucleation; electrocrystallization; electrodeposition; zinc-nickel, Schariffker and Hills model

Introduction

Zinc and its alloy coatings are finding numerous applications in different industries like automotive, electrical, aerospace *etc*., as sacrificial metallic coatings for the protection of steel components [1]. Zinc-nickel alloys obtained by electrodeposition process with the amount of nickel varying from 8 to 14 % by weight, facilitate corrosion protection and have other physical properties

five to six times superior to pure zinc coatings [2]. Amongst all commonly electroplated alloys, zinc-nickel alloy is the most commonly exploited alloy in commercial applications. This is due to its eco-friendly and economic nature as compared to toxic and expensive cadmium coatings [1]. Electrodeposition of Zn-Ni alloys is interesting, because these alloys exhibit significantly higher corrosion resistance and better surface morphology than pure zinc [3]. Although nickel is more noble metal than zinc, the co-deposition of zinc and nickel in Zn-Ni alloy is anomalous [4-5] and a higher percentage of zinc is present in the final deposit. According to Lin's conclusion, anomalous electrodeposition of zinc-nickel alloy is caused by the slow kinetics and hydrogen evolution at the nickel deposit. Zinc-nickel alloy provides a sacrificial protection to steel [6].

Many studies have been carried out to understand the characteristics of Zn-Ni alloy deposit. It has already been found that characteristics of the deposited coating depend on the applied voltage, current density, bath composition, pH, additives, temperature *etc*. The phases and the microstructure of the surface of deposited Zn-Ni alloy are other important characteristics which control the corrosion resistance and other mechanical properties [7]. Brighteners are often added into the plating bath solution of common metals such as zinc, nickel or cobalt to improve properties of the final deposit and to make the surface more durable, compact and uniform for better performance in terms of corrosion protection [3,8]. Brighteners are usually added into the electrolytic bath at very low concentration, in parts per million, but their presence in the bath promotes formation of smooth and shiny coatings [9].

Experimental

Bath solutions were freshly prepared using analytical grade chemicals in distilled water. The standard Hull cell of 267 ml capacity was used to optimize the bath constituents and bath variables. The Hull cell experiments were carried out without agitation [10]. pH value of the plating bath solution was measured using a digital pH-meter and adjusted with 10 % v/v H_2SO_4 or sodium bicarbonate solution. Zinc plate of 99.99 % purity was used as anode and activated each time by immersing in 10 % v/v HCl for 4-5 seconds, followed by washing with the running water. The mild steel plates of standard Hull cell size were mechanically polished to obtain smooth surfaces and degreased by dipping in the boiling trichloroethene. The scales and dust on the steel plates were removed by dipping in 10 % v/v HCl solution and then subjected to electro-cleaning process. Thereafter, steel plates were washed with distilled water, dried and then used for the experiments. After the experiment was finished, the plate was removed from the solution and subjected to bright dip in 1 % v/v HNO_3 solution for 3-5 seconds, followed by water washing and drying.

The condensation product was synthesized from equimolar amounts of salicylaldehyde (1 mM) with chemical formula C_7H_5O (AR grade, S.D fine chemicals) and cysteine hydrochloride (1 mM) with chemical formula $C_3H_{10}ClNO_3S$ in ethanol medium (50 ml) under reflux condition for 3 hours at 343 K [11]. The completion of the reaction was confirmed by thin layer chromatography (TLC). The resulting product was diluted to 100 ml with distilled water and a known amount of this solution was added to the plating bath solution. The bath solution was stirred for 30 min before conducting the experiments, in order to properly mix the condensation product with the plating bath solution.

The cyclic voltammetry and chronoamperometric studies were performed using CHI660D electrochemical workstation with a three-electrode system. A graphite electrode of geometrical area 0.02 cm^2, a platinum wire and a saturated calomel electrode (SCE) were used as the working, counter and reference electrodes respectively. Before conducting each experiment, the working electrode was polished to a mirror finish with 0.05 μm alumina.

The corrosion behavior of Zn-Ni alloy coatings obtained from the plating bath in presence and absence of SC were studied in 3.5 wt.% NaCl solution by galvanostatic polarization method and electrochemical impedance spectroscopic technique, using the electrochemical workstation (Instrument model CHI660D). A three-electrode assembly was used. The working electrode (WE), *i.e.* Zn-Ni coated mild steel plate was masked with a lacquer to expose 1 cm^2 area. A platinum foil was used as a counter electrode (CE) with saturated calomel as a reference electrode (RE). Polarization experiments were performed in the potential range between -0.9 V and -1.4 V at the scan rate of 0.01 V s^{-1}. Impedance spectra were measured with the perturbation signal amplitude of 0.005 V at frequencies between 100 kHz and 1 Hz.

The composition and surface morphology of deposits were analyzed using SEM images. X-ray diffraction studies were used to find the preferred orientation of Zn-Ni alloy crystallites and the phases present in the alloy deposit, both in presence and absence of SC. The X-ray diffractometer with a CuKα radiation was used to obtain XRD spectra. JCPDS powder diffraction file cards were used for phase identification.

The preferred orientation of the deposits was determined by Markesan's method, using the following equation for calculating the texture coefficient (T_c)

$$T_c = \frac{I(hkl)\sum I_o(hkl)}{\sum I(hkl)I_o(hkl)}100$$

(1)

where I(hkl) is the peak intensity of Zn-Ni electrodeposit and $\sum I$ is the sum of the intensities of independent peaks. The index 'o' refers to the intensities for the standard Zn-Ni sample (JCPDS 10-0209). The orientation with the maximum texture coefficient value is the preferred orientation of the Zn-Ni alloy crystallites in the deposit [12]. The percentage reflection of the deposit was determined using ocean optics USB 4000 spectrophotometer, referenced against a silver mirror. The reflectivity of silver mirror was set at 100 % and the measurements were carried out at different surface points of the deposited sample.

Results and discussion

Electrodeposition process

The bath constituents and operating conditions were optimised by Hull cell experiments to get a bright deposit over wide current density range [13]. The plating bath composed of zinc sulphate, nickel sulphate, sodium sulphate, cetyltrimethylammonium bromide (CTAB) and boric acid. Zinc sulphate and nickel sulphate were used as the main electrolytes, while sodium sulphate was used as an additional electrolyte which increased conductivity of the plating bath solution. CTAB was used as a wetting agent, while boric acid was added to improve the morphology, brightness and adhesion of the deposited nickel. From the available literature it has also been found that boric acid can act as a very good catalyst by lowering the over-voltage, what prefers deposition of nickel instead hydrogen evolution. Also, the literature revealed that boric acid plays an important role because it forms a complex, from which nickel can be, discharged more easily [14]. During the Hull cell experiments, a particular concentration at which good bright deposit is obtained was fixed as the optimum concentration. The procedure was repeated for all bath constituents and operating conditions. The optimized bath composition is given in Table 1. The basic bath gave coarse dull deposit within the current density range of 0.5 − 3 A dm^{-2}.The optimized bath solution gave mirror-bright deposit within the current density range of 1 − 6 A dm^{-2}.

Bath constituents	Concentration	Operating conditions
$ZnSO_4.7H_2O$	0.5 M	Anode: zinc plate (99.99 %)
$NiSO_4.6H_2O$	0.1 M	Cathode: mild steel plate
Na_2SO_4	0.29 M	pH 3.5
H_3BO_3	0.26 M	Temperature= 298 -303 K
CTAB	0.01 M	Plating time: 10 min
Brightener (SC)	40 ml L^{-1}	Bright current density range: 1-6 A dm^{-2}

Voltammetric response

Cyclic voltammetry was used to define the major characteristics of Zn-Ni alloy deposition process with and without SC as an additive. The results are shown in Figure 1.

In absence of SC during cathodic scan, the cathodic peak potential is placed at -1.17 V (E_1). This peak is associated with simultaneous reduction of both Zn^{2+} and Ni^{2+} ions to zinc and nickel atoms, respectively. On reversing the sweep direction, two current crossovers appear in the cathodic region. The more cathodic potential at which the crossover occurs is known as the nucleation overpotential (E_η) [13]. The second crossover at zero current region (-1.02 V) is known as crossover potential (E_{co}). Two crossovers are characteristic of three dimensional (3D) and subsequent crystal growth process. In the absence of SC in the optimized bath solution, four oxidation peaks (A_1, A_2, A_3 and A_4) are seen in the voltammogram.
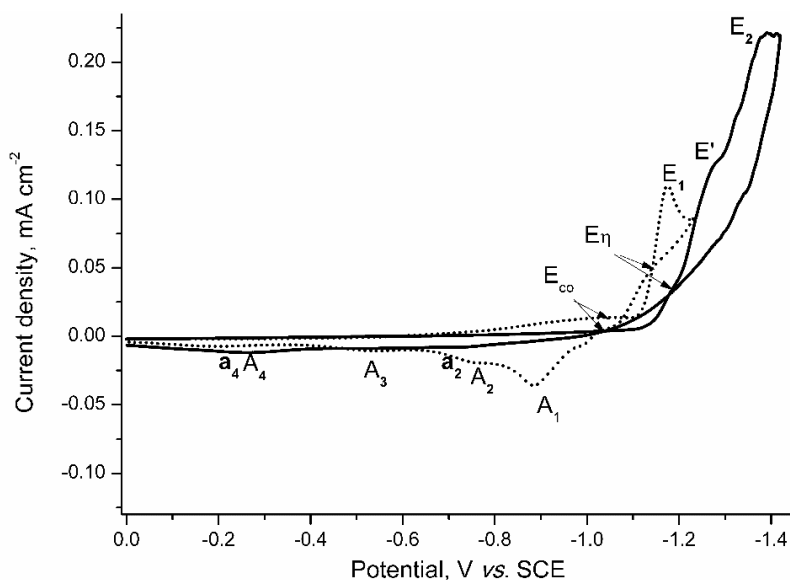
Figure1. *Typical cyclic voltammogram of Zn-Ni alloy coating deposited on graphite electrode from optimized zinc-nickel bath solution (Table 1), in presence (solid line) and absence (dotted line) of SC, in the potential range of 0 V to -1.42 V at scan rate of 0.05 Vs^{-1}*

The multiple peaks detected during the electrochemical oxidation of alloys are due to dissolution of metals in the alloy *via* different intermediate phases [13]. Four anodic dissolution peaks for Zn-Ni alloy correspond to the dissolution of three phases in zinc-nickel alloy deposit. They are η-phase (Zn), δ-phase (Ni_3Zn_{22}) and γ-phase (Ni_5Zn_{21}). The first anodic peak (A_1) at the potential of -0.89 V corresponds to the oxidation of zinc from the η-phase, which is almost pure zinc phase. The second (A_2) and the third (A_3) anodic peaks at potentials -0.76 V and -0.54 V respectively, correspond to dissolution of zinc from δ-phase and γ-phase respectively. The fourth anodic peak (A_4) at nobler potential (-0.27V) corresponds to the dissolution of nickel from η, δ and γ phases [3,9,15]. Thus, the voltammetric response gives information regarding the characteristics of the components of Zn-Ni

alloy and the structure of deposited phases. As also shown in Figure 1, in presence of SC, the plating bath cathodic potential (E_2) was shifted negatively to -1.41 V, which indicates that SC acts by adsorbing on the cathodic surface. Adsorbed SC created a barrier near the electrode surface that inhibits the discharge of metal ions, leading to a decrease in the grain size of the deposit [13]. The voltammogram in Figure 1 also shows two broad anodic peaks (a_2 and a_4) at -0.73V and -0.25 V. The first broad peak (a_2) corresponds to oxidation of zinc from the η-phase (zinc-rich phase) and the second broad peak (a_4) corresponds to the dissolution of nickel from η and γ phases. It can also be noticed that anodic peaks are slightly shifted to more positive potential in presence of SC. This indicated that oxidation of Zn-Ni alloy becomes more difficult due to the adsorption of SC and hence, the coating appears more smooth, compact and uniform. Similar results were observed in the literature [13].

Chronoamperometric analysis

Chronoamperometric analysis was performed to identify the nucleation mechanism at different potentials. The primary factor leading to the generation of fine-grained deposit is the formation of fresh nucleation sites and their growth rate. Chronoamperometric technique has proved to be a powerful way for explaining the mechanism of new phase formation (electrocrystallization process) [16]. For most of metals, the charge transfer rate is high, and the continuous growth of formed nuclei is entirely mass transfer controlled. According to the theory, two cases of nucleation can be considered based on the rate of nucleation. In the first case, at increased nucleation rate all nuclei are instantly formed after the potential step and their number remains constant during the growth process. This is called instantaneous nucleation and is described by the following equation:

$$j\,! = \left[\frac{zFD^{1/2}c}{(\pi t)^{1/2}} \right] \left[1 - \exp(-N\pi kDt) \right] \tag{2}$$

In eqn. (1), $j!$ = current density related to the geometric area of the electrode surface, N is the total number of nuclei formed, zF is the molar charge of the deposited species, D is the diffusion coefficient, c is the bulk concentration (mol dm^{-3}) and k is the numerical constant calculated from the following equation:

$$k = \left(\frac{8\pi cM}{\rho} \right)^{1/2} \tag{3}$$

In eqn. (3), M and ρ are the molar mass and metal density, respectively.

In the second type of nucleation, at decreased nucleation rate, the nuclei are continuously formed during the entire time, before overlapping of the diffusion hemispheres around the growing nuclei. This process is called progressive nucleation [16]. In this type of nucleation, the metal clusters of different sizes are formed, especially at the initial time (t). It is described by the following equation:

$$j! = \left\{ \left[\frac{zFD^{1/2}c}{(\pi t)^{1/2}} \right] \left[1 - \exp\left(\frac{-aN_{O}\pi k'Dt^2}{2} \right) \right] \right\} \tag{4}$$

In eqn. (4), N_o is the number density of substrate active sites, a is the steady state nucleation rate constant per site, while k' is the numerical constant and is given by:

$$k' = \frac{4}{3} \left(\frac{8\pi cM}{\rho} \right)^{1/2} \tag{5}$$

Figure 2 shows the current versus time (*I-t*) transients, recorded during metal reduction in the potential range from -1.12 to -1.18 V in absence of SC and -1.34 to -1.46 V in presence of SC in the plating bath. The transients exhibit the typical shape for a nucleation process with three-dimensional growth of nuclei limited by diffusion of the electroactive species [16]. At short times an increase in the current density is observed, corresponding to beginning and growth of the nuclei. At later stages, diffusion zones of adjacent nuclei overlap, and current density reaches a maximum followed by a decaying portion, converging to a limiting current corresponding to linear diffusion of electroactive ions to a planar electrode (Cottrell equation).
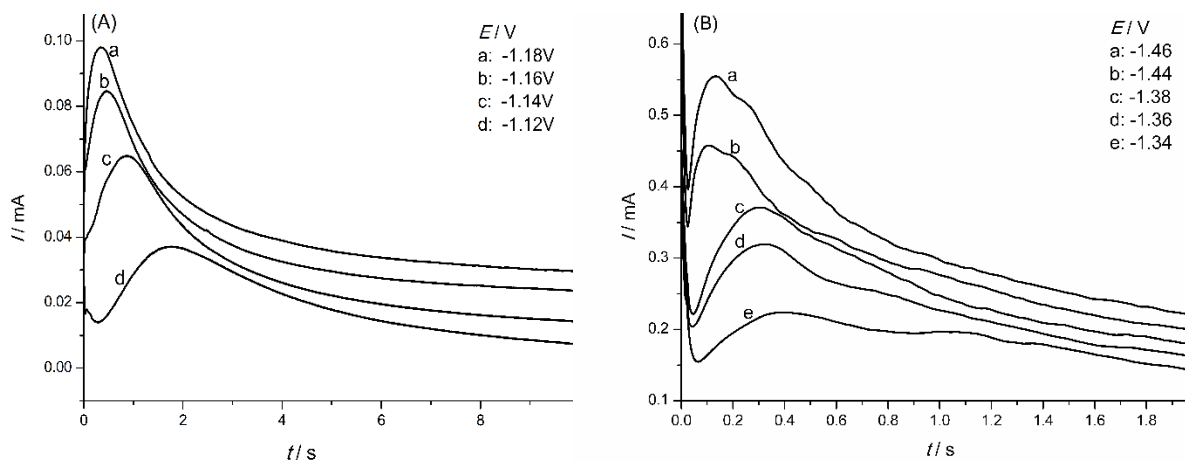
Figure 2. *Current transients for Zn-Ni deposition at different potentials from optimized plating bath solution (Table 1) in (A) absence and (B) presence of SC.*

The model of 3D nucleation with hemispherical diffusion control of the growing 3D clusters, describes the kinetics of phase formation of growing clusters of Zn-Ni alloy crystallites in early stages, when diffusion of the depositing species from the bulk of the solution to the electrode/solution interface is the slow step of the process, considering the eventual overlap of diffusion zones and the development of nucleation exclusion zones around already established nuclei [17].

Two limiting cases can be observed: *instantaneous nucleation* where all nuclei are formed immediately after the potential step and *progressive nucleation* where the number of nuclei increased during the whole deposition process. Different theoretical models of nucleation were developed and tested in the last two decades in order to predict the behavior of potentiostatic current transients. A convenient method to identify the nucleation mechanism was proposed by Schariffker and Hills [16]. The method is based on rendering the curves dimensionless by referencing the current, *I*, at any instant of time to the maximum current, I_{max}, and the time, *t*, to the time of maximum current, t_{max}. The following equations describe instantaneous eqn. (6) and progressive eqn. (7) nucleation:

$$\left(\frac{I}{I_{max}}\right)^2 = \frac{1.9542}{t/t_{max}}\left\{1-\exp\left[-1.2564\left(\frac{t}{t_{max}}\right)\right]\right\}^2 \tag{6}$$

$$\left(\frac{I}{I_{max}}\right)^2 = \frac{1.2254}{t/t_{max}}\left\{1-\exp\left[-2.3367\left(\frac{t}{t_{max}}\right)^2\right]\right\}^2 \tag{7}$$

Non-dimensional plots obtained using experimental and theoretical data for Zn-Ni alloy deposition in absence and presence of SC are shown in Figure 3 at different potentials.
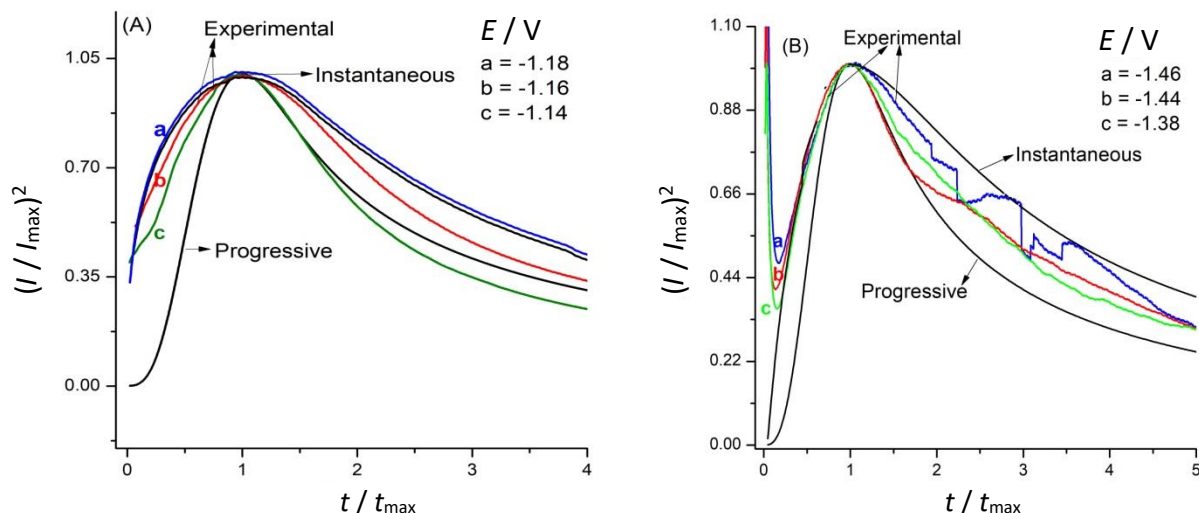
Figure 3. *Non-dimensional $(I/I_{max})^2$ vs. t/t_{max} plots for Zn-Ni deposition at different potentials from optimized plating bath solution (Table 1) in (A) absence and (B) presence of SC.*

The following mechanism explains the anomalous behaviour of Fe group metal ions on the electrode surface:

$$2H_2O + 2e^- \rightarrow H_2 + 2OH^- \tag{8}$$

$$M^{2+} + OH^- \rightarrow M(OH)^+ \tag{9}$$

$$M(OH)^+ \rightarrow M(OH)+_{ads} \tag{10}$$

$$M(OH)^+_{ads} + 2e^- \rightarrow M + OH^- \tag{11}$$

where M indicates nickel, iron and cobalt atoms. Although many attempts have been made to explain the anomalous co-deposition of alloys, there is still no universally accepted theory [18]. The reduction rate of M mainly depends on the stability of $M(OH)^+_{ads}$ or $M(OH)^+$. The stability of zinc and nickel metal mono hydroxide ions or metal hydroxides can be sorted in the following order: $Ni(OH)^+ > Zn(OH)^+$. As elucidated above, the amount of nickel in the deposit is much lower than in the plating bath solution. Also, the concentration of nickel ions near the cathode surface should be maintained at a constant value during the entire electroplating process [9]. The nucleation process of Zn-Ni deposit is always associated with release of hydrogen which is seen from equation (8). Hence the experimental $(I/I_{max})^2$ should be much larger than the theoretical model [3].

As seen in Figure 3(A), in absence of SC, the rising part of the transients are located near the instantaneous nucleation curve at lower potentials. In presence of SC shown in Figure 3(B), the normalized curves are located on the theoretical instantaneous nucleation curve under studied potentials. This result confirmed 3D instantaneous nucleation mechanism of Zn-Ni alloy deposition in presence of SC.

Another diagnostic criterion given by Schariffker and Hills nucleation model is based on the rising part of the current-time transient curve, which is in fact the analysis of initial stage of deposition [16]. It is possible to represent I versus $t^{1/2}$ for instantaneous and I versus $t^{3/2}$ for progressive nucleation. Based on this model, I versus $t^{1/2}$ for instantaneous nucleation are shown in Figure 4.

Figure 4(A) shows linearly fitted plots of I vs. $t^{1/2}$ in absence of SC, which indicate that at higher negative potentials the nucleation occurs by instantaneous nucleation mechanism. In Figure 4(B), linearity is also obtained for all I vs. $t^{1/2}$ plots, which indicates that even in presence of SC, the nucleation continues to occur by instantaneous mechanism at all studied potentials.
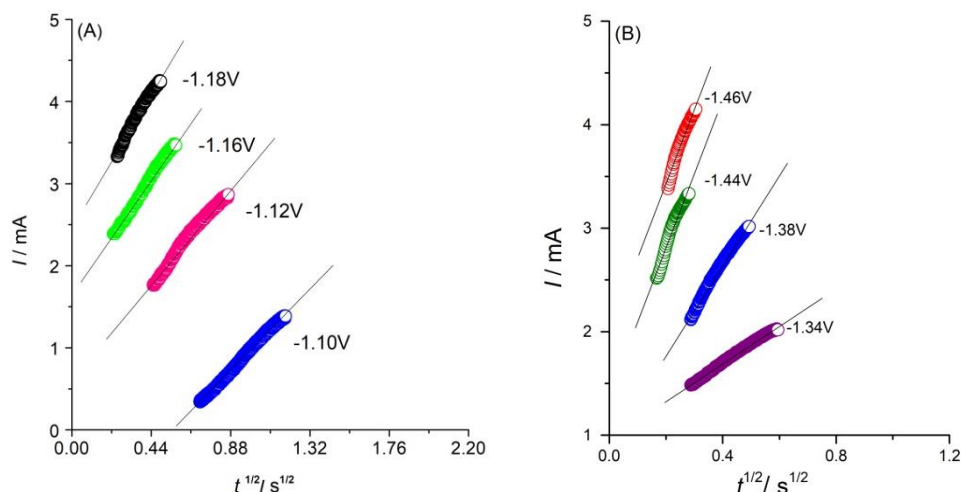
Figure 4. I vs. t$^{1/2}$ plots for initial transient portions of Zn-Ni deposition at different potentials in (A) absence of SC and (B) presence of SC. Data are taken from Figures 2A and 2B.

Impedance and polarization studies

Corrosion resistance studies were carried out in 3.5 wt.% NaCl electrolyte solution using electrochemical impedance spectroscopy (EIS) and polarization (Tafel extrapolation method) techniques. The results are presented in Figure 5.
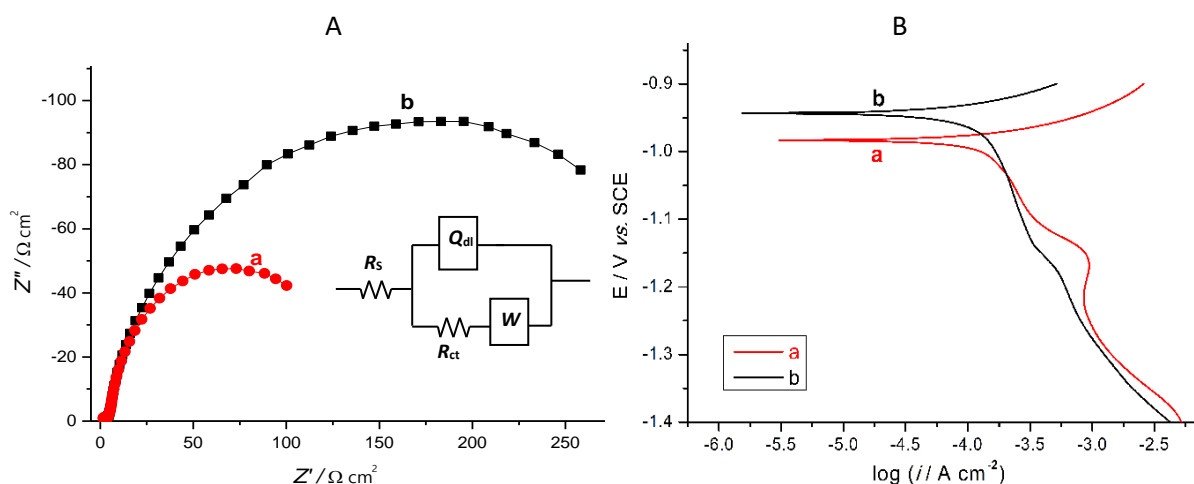
Figure 5.(A) Nyquist Impedance plots and **(B)** Tafel polarization curves in the potential range -0.8V to -1.4V and scan rate 0.01Vs^{-1} of Zn-Ni coatings on mild steel in 3.5 wt. % NaCl solution. Zn-Ni electrodeposits are obtained in **a** absence and **b** presence of SC in the optimized plating bath solution (Table 1). Inset in Fig. 5(A) shows electrical equivalent circuit used to simulate measured EIS data.

Nyquist plots of Zn-Ni deposits obtained in absence and presence of SC in the optimized bath are compared in Figure 5(A). The charge transfer resistance values of deposits prepared in absence and presence of SC were calculated with the help of ZSimpWin 3.21 software as 164 and 313 Ω cm^2. This revealed that the bright coating increased the corrosion resistance of mild steel substrate, what is in good agreement with the polarization results shown in Figure 5(B) obtained for dull and bright coatings on mild steel substrate. Polarization data revealed decrease in $I_{corr.}$ value from 73.11 μA cm^{-2} (dull deposit) to 10.16 μA cm^{-2} (bright deposit). Also, in presence of SC, $E_{corr.}$values are shifted to nobler direction, indicating reduction in corrosion rate and thereby increase in the corrosion resistance.

These results suggest that the bright deposit can successfully act as a protective layer for mild steel substrate and can also improve the corrosion resistance of the decorative bright coating.

Surface morphology - SEM analysis and reflectance studies

Figure 6 shows the SEM images of Zn-Ni alloy electrodeposits obtained in absence and presence of SC in the optimized bath solution. The deposit obtained in absence of SC shows coarse grained structure having randomly distributed crystallites, whereas the bright deposit shows fine-grained, uniform, smooth and compact deposit. This indicates that SC promotes grain refinement by increasing the number of nucleation sites and retarding the random growth of nuclei during deposition.
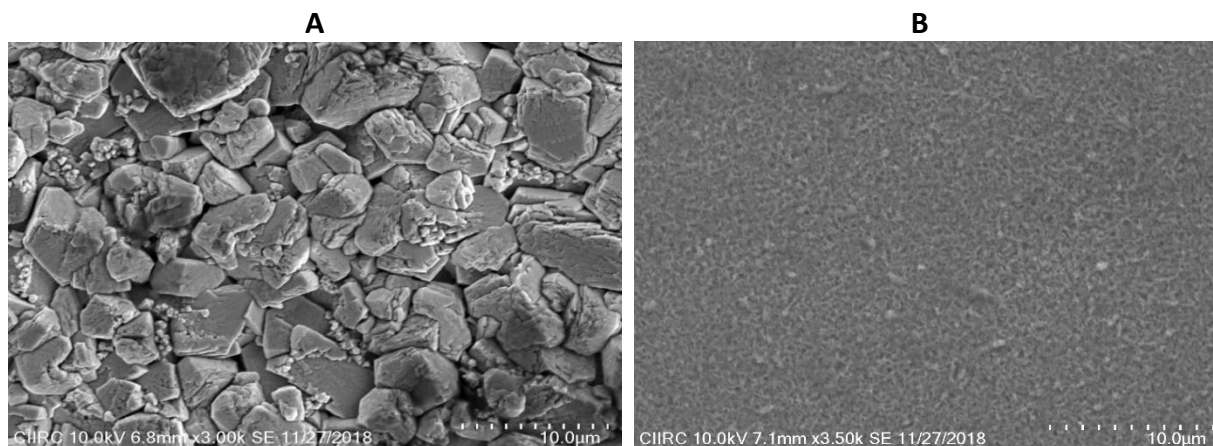
Figure 6. *SEM images of Zn-Ni coatings electrodeposited at 4 Adm^{-2} from the optimized plating bath solution (Table 1) in (A) absence and (B) presence of SC*

The ideal reflectance and the degrees of total reflection as a function of wavelength of visible light for Zn-Ni alloy electrodeposits formed in presence and absence of SC are shown in Figure 7. From the reflectance spectra, it is observed that bright deposits obtained in presence of SC in plating bath increases percentage of reflection in the visible region. This result confirmed that SC acts as a good brightener for Zn-Ni alloy coatings.
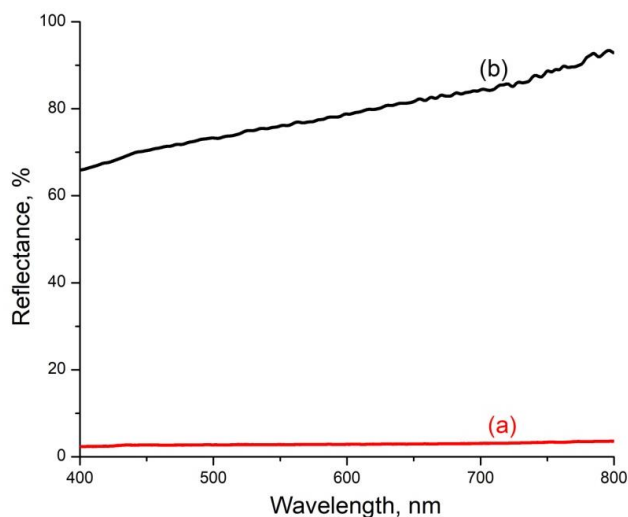
Figure 7. *Reflectance spectra of Zn-Ni coatings electrodeposited at mild steel electrode at 4 A dm^{-2} from the optimized plating bath solution (Table 1) in (a) absence and (b) presence of SC*

X-ray Diffraction Analysis

XRD patterns of dull and bright Zn-Ni alloy deposits are presented in Figure 8, showing formation of lines corresponding to η-phase Zn (101) and additional lines that can be indexed considering a γ-Ni$_5$Zn$_{21}$ phase. All peaks correspond exclusively to zinc metal and zinc-nickel alloy, which means that there are no impurities in the deposit. It is also observed that there is an increase of the intensity γ-Ni$_5$Zn$_{21}$ phase line obtained in presence of SC in the plating bath solution. This increase in the intensity is due to the increase in percentage of nickel.
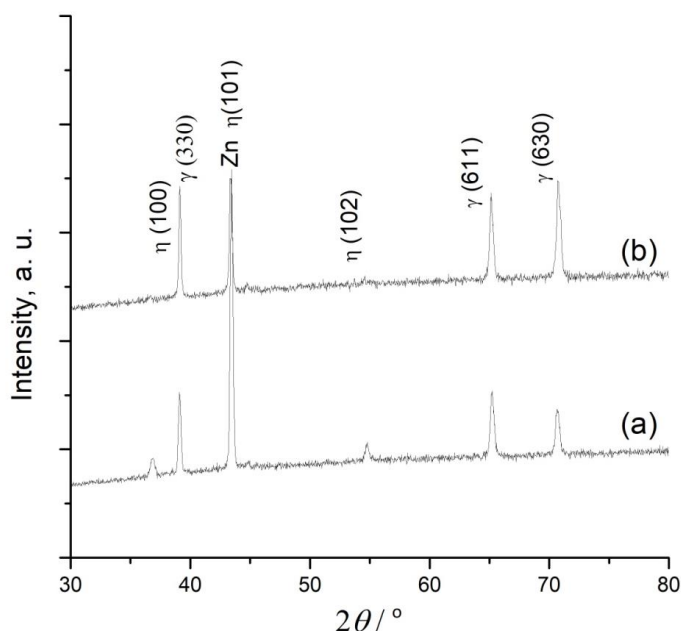
Figure 8. *X-ray diffraction patterns of Zn-Ni electrodeposits observed in (a) absence and (b) presence of SC in the optimized plating bath solution (Table 1)*

To know the preferred orientation of Zn-Ni alloy deposit, the texture coefficient was calculated for each peak in diffraction patterns. In dull deposit, the texture coefficient value was found to be maximum for (611) plane. Hence (611) was the preferred orientation of the crystallites in dull deposit. In the case of bright deposit, the texture coefficient value was maximum for (630) plane. Hence (630) was the preferred orientation of the crystallites in bright deposit. The adsorption of SC on different plane, changes the preferred orientation of the crystallites in the deposit from (611) to (630), which in turn alters the surface morphology of the deposit and thereby improves the corrosion resistant property.

Conclusions

The newly synthesized brightener (SC) gives smooth, uniform, fine-grained and mirror-bright Zn-Ni alloy coating electrodeposited from the optimized plating bath solution. The voltammetric response gives information regarding the components of the deposit and structure of deposited phases present in Zn-Ni alloy coating in presence and absence of SC. The chronoamperometric studies revealed that the mechanism of Zn-Ni alloy electrodeposition in presence of SC follows three dimensional (3D) instantaneous nucleation mechanism. Corrosion studies confirmed that presence of SC in the plating bath improves corrosion resistance and hence protection ability of Zn-Ni alloy coating. SEM and reflectance studies also confirmed that the presence of SC in zinc-nickel plating bath promotes the formation of smooth, shiny, compact and corrosion resistant coating. The performed studies suggest that the newly synthesized brightener (SC) can be conveniently used as a brightener in decorative applications and also for increasing the corrosion resistance of steel components in engineering and electroplating applications.

Availability of data and materials – The data used and analyzed during the current study are available from the corresponding author on reasonable request.

References

[1]   S. Rashmi, L. Elias, A. C. Hegde, *Engineering Science & Technology* **20** (2017) 1227-1232.
https://doi.org/10.1016/j.jestch.2016.10.005

[2]   S. B. Ramesh, K.U. Bhat, A.C. Hegde, *Analytical& Bioanalytical Electrochemistry* **3** (2011) 302-315.

[3]   S. Basavanna, Y. A. Naik, *Journal of Applied Electrochemistry* **39** (2009) 1975-1982.
https://doi.org/10.1007/s10800-009-9907-1

[4]   Z. Feng, Q. Li, J. Zhang, P. Yang, *Journal of the Electrochemical Society* **162** (2015) D412-D422.
http://jes.ecsdl.org/content/162/9/D412.full

[5]   A. Brenner, *Electrodeposition of alloys, principles and practice*; Academic press, New York **1** (1963)
E-Book ISBN: 9781483223117.

[6]   C. A. M. Dutra, J. W. J. Silva, R. Z. Nakazato, *Materials Sciences and Applications* **4** (2013) 644-648.
https://file.scirp.org/Html/9-7701149_38134.htm

[7]   M. J. Rahman, S.R. Sen, M. Moniruzzaman, *Journal of Mechanical Engineering* **40** (2009) 9-14.
http://citeseerx.ist.psu.edu/viewdoc/download?doi=10.1.1.619.2785&rep=rep1&type=pdf

[8]   Y. A. Naik, T.V. Venkatesha, *Bulletin of Material Science* **28** (2005) 495-501.
https://doi.org/10.1007/BF02711243

[9]   S. Basavanna, Y. A. Naik, *Journal of Applied Electrochemistry* **41** (2011) 535-541.
https://doi.org/10.1007/s10800-011-0263-6

[10] S. Basavanna, Y. A. Naik, *Indian Journal of Chemical Technology* **19** (2012) 91-95.
http://nopr.niscair.res.in/handle/123456789/13703

[11] D. Chen, A. E. Martell, *Inorganic Chemistry*, **26**(1987) 1026-1030.
https://doi.org/10.1021/ic00254a013

[12] L. P. Berube, G.L. Esperance, *Journal of Electrochemical Society* **136** (1989) 2314-2328.
http://jes.ecsdl.org/content/136/8/2314.abstract

[13] K. O. Nayana, T. V. Venkatesha, *Bulletin of Material Science* **37**(2014) 1137-1146.
https://www.ias.ac.in/article/fulltext/boms/037/05/1137-1146

[14] Y. Addi, A. Khouider, *International Journal of Electrochemistry* **2011** (2011) 1-7.
http://dx.doi.org/10.4061/2011/742191

[15] M. M. Abou-Krisha, *Applied Surface Science* **252** (2005) 1035-1048.
https://doi.org/10.1016/j.apsusc.2005.01.161

[16] B. R. Schariffker, G. Hills, *Electrochimica Acta* **28** (1983) 879-889.

[17] A. E. Alvarez, D. R. Salinas, *Journal of Electroanalytical Chemistry* **566** (2004) 393-400.
https://doi.org/10.1016/j.jelechem.2003.11.051

[18] A. Bai, C. C. Hu, *Electrochimica Acta* **50** (2005) 1335–1345.
https://doi.org/10.1016/j.electacta.2004.07.055